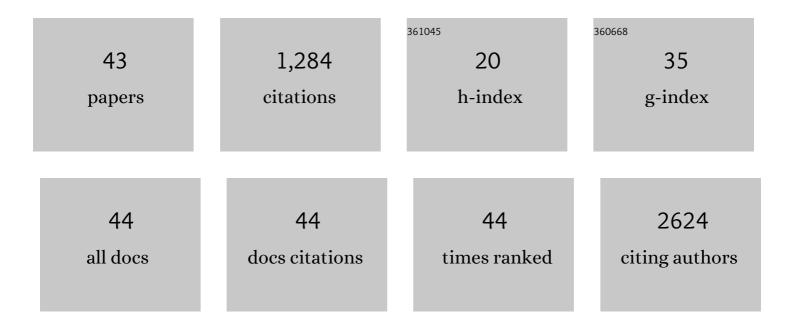
## MarÃa Collantes

List of Publications by Year in descending order

Source: https://exaly.com/author-pdf/7737245/publications.pdf Version: 2024-02-01



#	Article	IF	CITATIONS
1	Oral Immunogenicity of Enterotoxigenic Escherichia coli Outer Membrane Vesicles Encapsulated into Zein Nanoparticles Coated with a Gantrez® AN–Mannosamine Polymer Conjugate. Pharmaceutics, 2022, 14, 123.	2.0	4
2	Cerebral metabolic pattern associated with progressive parkinsonism in non-human primates reveals early cortical hypometabolism. Neurobiology of Disease, 2022, 167, 105669.	2.1	5
3	Preclinical safety of negatively charged microspheres (NCMs): Optimization of radiolabeling for in vivo and ex vivo biodistribution studies after topical administration on full-thickness wounds in a rat model. European Journal of Pharmaceutics and Biopharmaceutics, 2022, 177, 61-67.	2.0	2
4	In vivo SPECT-CT imaging and characterization of technetium-99m-labeled bevacizumab-loaded human serum albumin pegylated nanoparticles. Journal of Drug Delivery Science and Technology, 2021, 64, 101809.	1.4	8
5	Changes in brown adipose tissue lipid mediator signatures with aging, obesity, and DHA supplementation in female mice. FASEB Journal, 2021, 35, e21592.	0.2	18
6	Glucocerebrosidase Gene Therapy Induces Alpha-Synuclein Clearance and Neuroprotection of Midbrain Dopaminergic Neurons in Mice and Macaques. International Journal of Molecular Sciences, 2021, 22, 4825.	1.8	18
7	mRNA-based therapy in a rabbit model of variegate porphyria offers new insights into the pathogenesis of acute attacks. Molecular Therapy - Nucleic Acids, 2021, 25, 207-219.	2.3	7
8	Engineering a genomeâ€reduced bacterium to eliminate <i>Staphylococcus aureus</i> biofilms <i>inÂvivo</i> . Molecular Systems Biology, 2021, 17, e10145.	3.2	21
9	ld1 and PD-1 Combined Blockade Impairs Tumor Growth and Survival of KRAS-mutant Lung Cancer by Stimulating PD-L1 Expression and Tumor Infiltrating CD8+ T Cells. Cancers, 2020, 12, 3169.	1.7	10
10	In vivo efficacy of bevacizumab-loaded albumin nanoparticles in the treatment of colorectal cancer. Drug Delivery and Translational Research, 2020, 10, 635-645.	3.0	22
11	Preclinical safety of topically administered nanostructured lipid carriers (NLC) for wound healing application: biodistribution and toxicity studies. International Journal of Pharmaceutics, 2019, 569, 118484.	2.6	28
12	Inhibitor of Differentiation-1 Sustains Mutant <i>KRAS</i> -Driven Progression, Maintenance, and Metastasis of Lung Adenocarcinoma via Regulation of a FOSL1 Network. Cancer Research, 2019, 79, 625-638.	0.4	19
13	Assessment of metabolic patterns and new antitumoral treatment in osteosarcoma xenograft models by [18F]FDG and sodium [18F]fluoride PET. BMC Cancer, 2018, 18, 1193.	1.1	11
14	Non-invasive in vivo imaging of cardiac stem/progenitor cell biodistribution and retention after intracoronary and intramyocardial delivery in a swine model of chronic ischemia reperfusion injury. Journal of Translational Medicine, 2017, 15, 56.	1.8	24
15	The inhibitor of differentiation-1 (Id1) enables lung cancer liver colonization through activation of an EMT program in tumor cells and establishment of the pre-metastatic niche. Cancer Letters, 2017, 402, 43-51.	3.2	36
16	Lessons from 11C-dihydrotetrabenazine imaging in a xenograft mouse model of rat insulinoma: is PET imaging of pancreatic beta cell mass feasible?. Quarterly Journal of Nuclear Medicine and Molecular Imaging, 2017, 61, 447-455.	0.4	1
17	Index lesion characterization by <sup>11</sup> C holine PET/CT and Apparent Diffusion Coefficient parameters at 3 Tesla MRI in primary prostate carcinoma. Prostate, 2016, 76, 3-12.	1.2	9
18	Glucose metabolism during fasting is altered in experimental porphobilinogen deaminase deficiency. Human Molecular Genetics, 2016, 25, 1318-1327.	1.4	19

MARÃA COLLANTES

#	Article	IF	CITATIONS
19	Radiation dosimetry and biodistribution in non-human primates of the sodium/iodide PET ligand [18F]-tetrafluoroborate. EJNMMI Research, 2015, 5, 70.	1.1	14
20	Infiltration of plasma rich in growth factors enhances in vivo angiogenesis and improves reperfusion and tissue remodeling after severe hind limb ischemia. Journal of Controlled Release, 2015, 202, 31-39.	4.8	52
21	Meox2/Tcf15 Heterodimers Program the Heart Capillary Endothelium for Cardiac Fatty Acid Uptake. Circulation, 2015, 131, 815-826.	1.6	88
22	Monoaminergic PET imaging and histopathological correlation in unilateral and bilateral 6-hydroxydopamine lesioned rat models of Parkinson's disease: A longitudinal in-vivo study. Neurobiology of Disease, 2015, 77, 165-172.	2.1	19
23	Functional MMPâ€10 is required for efficient tissue repair after experimental hind limb ischemia. FASEB Journal, 2015, 29, 960-972.	0.2	19
24	<i>In Vivo</i> Monitoring of Staphylococcus aureus Biofilm Infections and Antimicrobial Therapy by [ <sup>18</sup> F]Fluoro-Deoxyglucose–MicroPET in a Mouse Model. Antimicrobial Agents and Chemotherapy, 2014, 58, 6660-6667.	1.4	17
25	Levodopa induces long-lasting modification in the functional activity of the nigrostriatal pathway. Neurobiology of Disease, 2014, 62, 250-259.	2.1	8
26	Splicing regulator SLU7 is essential for maintaining liver homeostasis. Journal of Clinical Investigation, 2014, 124, 2909-2920.	3.9	55
27	The nigrostriatal system in the presymptomatic and symptomatic stages in the MPTP monkey model: A PET, histological and biochemical study. Neurobiology of Disease, 2012, 48, 79-91.	2.1	93
28	MAPC Transplantation Confers a more Durable Benefit than AC133+ Cell Transplantation in Severe Hind Limb Ischemia. Cell Transplantation, 2011, 20, 259-270.	1.2	28
29	Radiation protection in an animal research unit with pet: Occupational doses and dose rates produced by animals. Radiation Measurements, 2011, 46, 1307-1309.	0.7	2
30	Molecular Imaging Techniques to Study the Biodistribution of Orally Administered 99mTc-Labelled Naive and Ligand-Tagged Nanoparticles. Molecular Imaging and Biology, 2011, 13, 1215-1223.	1.3	29
31	Statistical parametric maps of 18F-FDG PET and 3-D autoradiography in the rat brain: a cross-validation study. European Journal of Nuclear Medicine and Molecular Imaging, 2011, 38, 2228-2237.	3.3	29
32	Adeno-Associated Virus Liver Transduction Efficiency Measured by <i>in Vivo</i> [ <sup>18</sup> F]FHBG Positron Emission Tomography Imaging in Rodents and Nonhuman Primates. Human Gene Therapy, 2011, 22, 999-1009.	1.4	14
33	Transplantation of Mesenchymal Stem Cells Exerts a Greater Long-Term Effect than Bone Marrow Mononuclear Cells in a Chronic Myocardial Infarction Model in Rat. Cell Transplantation, 2010, 19, 313-328.	1.2	70
34	Progression of dopaminergic depletion in a model of MPTP-induced Parkinsonism in non-human primates. An 18F-DOPA and 11C-DTBZ PET study. Neurobiology of Disease, 2010, 38, 456-463.	2.1	66
35	Antitumor and antiangiogenic effect of the dual EGFR and HER-2 tyrosine kinase inhibitor lapatinib in a lung cancer model. BMC Cancer, 2010, 10, 188.	1.1	61
36	Intensive Pharmacological Immunosuppression Allows for Repetitive Liver Gene Transfer With Recombinant Adenovirus in Nonhuman Primates. Molecular Therapy, 2010, 18, 754-765.	3.7	31

MARÃA COLLANTES

#	Article	IF	CITATIONS
37	Deletion of Inducible Nitric-Oxide Synthase in Leptin-Deficient Mice Improves Brown Adipose Tissue Function. PLoS ONE, 2010, 5, e10962.	1.1	46
38	PET imaging of thymidine kinase gene expression in the liver of non-human primates following systemic delivery of an adenoviral vector. Gene Therapy, 2009, 16, 136-141.	2.3	15
39	New MRI, 18F-DOPA and 11C-(+)-α-dihydrotetrabenazine templates for Macaca fascicularis neuroimaging: Advantages to improve PET quantification. NeuroImage, 2009, 47, 533-539.	2.1	24
40	Transplantation of adipose derived stromal cells is associated with functional improvement in a rat model of chronic myocardial infarction. European Journal of Heart Failure, 2008, 10, 454-462.	2.9	188
41	13N-Ammonia PET as a Measurement of Hindlimb Perfusion in a Mouse Model of Peripheral Artery Occlusive Disease. Journal of Nuclear Medicine, 2007, 48, 1216-1223.	2.8	20
42	Simple automated system for simultaneous production of 11C-labeled tracers by solid supported methylation. Applied Radiation and Isotopes, 2006, 64, 808-811.	0.7	22
43	Distribution of adrenomedullin and proadrenomedullin N-terminal 20 peptide immunoreactivity in the pituitary gland of the frog Rana perezi. General and Comparative Endocrinology, 2003, 133, 50-60.	0.8	9